RSC Advances

PAPER

View Article Online
View Journal | View Issue

Cite this: *RSC Adv.*, 2025, **15**, 5151

Rosé or white, glass or plastic: computer vision and machine learning study of cavitation bubbles in sparkling wines

Timur Aliev, [a] Ilya Korolev, [a] Mikhail Yasnov,[a] Michael Nosonovsky *[b] and Ekaterina V. Skorb [a]

This study presents a machine learning (ML)/Artificial Intelligence (AI) approach to classify types of sparkling wines (champagnes) and their respective containers using image data of bubble patterns. Sparkling wines are oversaturated with dissolved CO_2, which results in extensive bubbling when the wine bottle is uncorked. The nucleation and properties of bubbles depend on the chemical composition of the wine, the properties of the glass, and the concentration of CO_2. For carbonated liquids supersaturated with CO_2, the interaction of natural and cavitation bubbles is a non-trivial matter. We study ultrasonic cavitation bubbles in two types of sparkling wines and two types of glasses with the computer vision (CV) analysis of video images and clustering using an artificial neural network (NN) approach. By integrating a segmentation NN to filter out irrelevant frames and applying the Contrastive Language-Image Pre-Training (CLIP) NN for feature embedding, followed by TabNet for classification, we demonstrate a novel application of ML/AI for distinguishing champagne characteristics. The results show that the bubbles are significantly different to be classified by the ML techniques for different types of wine and glasses. Consequently, our study demonstrates that CV/AI/ML analysis of ultrasound cavitation bubbles can be used to analyze carbonated liquids.

Received 2nd January 2025
Accepted 6th February 2025

DOI: 10.1039/d5ra00046g

rsc.li/rsc-advances

Introduction

Champagne or sparkling wine is a popular alcoholic beverage originating from France's Champagne region. The global sparkling wine market was valued at $33.9 billion in 2019 and is anticipated to reach $51.7 billion by 2027.[1] Consequently, champagne quality and attractiveness to customers is a very important issue.

Bubbles in Champagne and sparkling wine have been studied by many researchers.[2–10] Sparkling wine is supersaturated with carbon dioxide (CO_2), whose partial pressure in the bottleneck is about $P = 5$–7 atm at 20 °C. The total amount of dissolved CO_2 in a standard 0.75 L bottle is close to 9 g, which corresponds to about 5 L volume of gaseous CO_2 under standard conditions. Due to the presence of alcohol, wine's surface tension is about $\gamma \approx 50$ mN m^{-1} (pure water has $\gamma \approx 72$ mN m^{-1}) and its viscosity is about 50% larger than that of pure water.[4,5] The critical radius of bubble nucleation is given by the Laplace equation as

$$R_{cr} = \frac{2\gamma}{P} \approx \frac{2 \times 0.05}{5 \times 10^5} = 0.2\ \mu\text{m} \quad (1)$$

The quality control of liquids by the analyses of visual images of ultrasonically induced cavitation bubbles is a relatively new method of non-destructive quality control, which has been applied to various liquids including water–ethanol solutions and petroleum products.[11–16]

During the ultrasound cavitation, bubbles of dissolved gas and vapors of the solvent itself form due to localized pressure changes caused by ultrasound. The size of bubbles oscillates due to the ultrasonic acoustic excitation, which causes compressive and tensile stress. At the compressive phase, bubbles shrink, while at the tensile phase, they expand for the amount that exceeds shrinking thus resulting in the growth of the average bubble radius.

While behavior close to the instability is difficult to predict by traditional deterministic methods, oscillating and collapsing bubbles can provide large amounts of datasets (*e.g.*, visual images), which makes them an almost ideal object for Artificial Intelligence (AI) and Machine Learning (ML) analyses and searches for correlations in data. Artificial Neural Network (ANN) was trained to determine the composition (alcohol concentration) of these solutions based on the bubble images.[11] Besides the ultrasonic cavitation, ML/AI and other novel computational methods are widely used to analyze the taste quality of food products such as the bitter taste in wines[17] and the umami taste in various products.[18]

[a]*Infochemistry Scientific Center, ITMO University, 9 Lomonosov St., St. Petersburg, 191002, Russia*

[b]*Department of Mechanical Engineering, University of Wisconsin-Milwaukee, N Cramer St. 3200, Milwaukee, WI 53211, USA. E-mail: nosonovs@uwm.edu*

In water–ethanol solutions, the shape and evolution of microbubbles is sensitive to the viscosity and surface tension, which are dependent on the ethanol concentration. Using a large amount of data (bubble images obtained from video recording) it is possible to determine solution concentrations by Machine Learning (ML) algorithms.[11]

Applying a similar approach to carbonated beverages such as sparkling wine is more challenging for two reasons. First, alcohol concentration does not vary significantly in different sorts of wine. The difference in the chemical composition of different types of wine is often a fraction of a percent, and, therefore, it does not always affect properties significant for bubbles, such as surface tension and viscosity. Second, sparkling wine is oversaturated with carbon dioxide, generating a large amount of CO_2 bubbles even without ultrasonic cavitation. These natural bubbles' behavior may differ from that of cavitation bubbles. The interaction of the bubbles formed in the supersaturated carbonated beverage with the bubbles induced by ultrasound cavitation is a non-trivial matter. It is therefore desirable to study the feasibility of the ultrasonic cavitation method for sparkling wine classification. It is known also that the behavior of bubbles in sparkling wine depends on the surface properties of the glass. It may also depend on the time since uncorking. These factors introduce additional variables that should be considered.

In this study, we will apply the Computer Vision (CV) methods to the visual recordings of cavitation bubbles in two sorts of sparkling wine kept for certain time intervals after the uncorking of the bottle in a glass and plastic cups. After that, ML methods will be applied by training a Contrastive Language-Image Pre-Training (CLIP) Artificial Neural Network (ANN) to cluster and classify data points corresponding to different samples. The data for sparkling wines will be compared with the data for water-alcohol solutions with similar alcohol concentrations.

Bubbles in sparkling wines

In this section, we review the physics of sparkling wine bubbles and will formulate hypotheses for which the ML analysis is sought.

Sparkling wine composition and properties significant for bubbles

From a chemist's point of view, sparkling wine is a multicomponent hydroalcoholic solution consisting of 93–97% water and alcohol (usually about 12.5%). The remaining 3–7% constitute sugar (1–5%), tartaric, malic, and lactic acids (0.6–0.8%) resulting in pH $\approx$ 3.0–3.2, and some glycerol (0.5%). Besides that, wine contains small (<g L^{-1}) concentrations of organic compounds, mineral ions, proteins, glycoproteins, polysaccharides, polyphenols, and volatile aromatic substances (Table 1). The presence of alcohol reduces the surface tension of wine down to about $\gamma \approx 50$ mN m^{-1} from that of pure water at room temperature, $\gamma \approx 72$ mN m^{-1}. The wine viscosity is about 50% larger than that of pure water,[4,5] Table 1. The color of wine is usually dependent on the anthocyanin pigments, which give wine the red color. The typical concentrations are on the order of 140–880 mg L^{-1}.[19] We do not have any direct evidence or data on anthocyanin's effect on the physico-chemical properties of wine.

Table 1 Typical composition of Champagne wine (based on ref. 2)

Compound	Concentration
Ethanol (C_2H_5OH)	$\approx$12.5%
Sugars (*e.g.* $C_6H_{12}O_6$)	10–50 g L^{-1}
CO_2	10–12 g L^{-1}
Glycerol ($C_3H_8O_3$)	$\approx$5 g L^{-1}
Tartaric acid ($C_4H_6O_6$)	2.5–4 g L^{-1}
Lactic acid ($C_3H_6O_3$)	$\approx$4 g L^{-1}
Volatile organic compounds	$\approx$0.7 g L^{-1}
K^+	0.2–4.5 g L^{-1}
Ca^{2+}	0.06–0.12 mg L^{-1}
SO_4^{2-}	0.2 mg L^{-1}
Polysaccharides	$\approx$0.2 mg L^{-1}
Polyphenols	$\approx$0.1 g L^{-1}
Mg^{2+}	0.05–0.09 g L^{-1}

Concentration of CO_2 in sparkling wines

The traditional method of sparkling wine production (*méthode champenoise*) involves two stages of fermentation. During the primary fermentation stage, grapes (traditionally, Chardonnay, Pinot Meunier, and Pinot Noir), are mixed and pressed, after which yeast (*Saccharomyces cerevisiae* fungus) is added to facilitate alcoholic fermentation. The latter is the chemical reaction of conversion of sugars into ethanol and carbon dioxide

$$C_6H_{12}O_6 \rightarrow 2CH_3CH_2OH + 2CO_2 \quad (2)$$

The second stage of fermentation, referred to as *prise de mousse*, occurs in cool cellars at temperatures between 12 °C and 14 °C. Wine is kept in tightly closed bottles along with added sugar and yeast. At this stage, wine becomes saturated with CO_2. The concentration of dissolved CO_2 is proportional to its partial pressure in the vapor phase, which, in turn, is proportional to the amount of added sugar. Sparkling wine is supersaturated with CO_2, whose partial pressure in the bottleneck is about 5–7 atm at 20 °C. The total amount of dissolved CO_2 in a standard 0.75 L bottle is close to 9 g, which corresponds to about 5 L volume of gaseous CO_2 under standard conditions for temperature and pressure.

During the secondary fermentation, the concentration of CO_2 in wine is in equilibrium with the partial vapor pressure P_{CO_2} in is given by Henry's law

$$c = k_H P_{CO_2} \quad (3)$$

where k_H is the Henry's law constant.[2] The temperature dependency of the constant is often expressed by the Van't Hoff equation as

$$k_H(T) = k_{298K}\exp\left[-\frac{\Delta H_{diss}}{R}\left(\frac{1}{T}-\frac{1}{298}\right)\right] \quad (4)$$

where $\Delta H_{diss} \approx 24\,800$ J mol^{-1} is the dissolution enthalpy of CO_2, $R = 8.31$ J (K mol)$^{-1}$ is the ideal gas constant. The value of k_H changes between $k_H = 2.98$ kg m^{-3} atm^{-1} at $T = 0$ °C and $k_H = 1.21$ kg m^{-3} atm^{-1} at $T = 25$ °C.[2,3]

The temperature-dependency of the gas pressure in the bottle can be calculated by combining Henry's law with the ideal gas state law, and it was estimated by Liger-Belair *et al.*[3] as

$$P_{CO_2}(T) \approx \frac{mRT}{4400V_G + k_H(T)RTV_L} \quad (5)$$

where M is the mass of CO_2 in the bottle in grams, V_L and V_G are the volumes of liquid and gas in the bottle in liters.[2] At typical values of $V_L = 0.75$ L, $V_G = 0.025$ L, $m = 9$ g (based on 24 g L^{-1} of sugar), and $T = 10$ °C, eqn (5) yields the pressure value close to $P_{CO_2} = 5$ atm.

Effect of uncorking the bottle

A large amount of CO_2 dissolved in wine results in extensive bubbling and sparkling after a bottle of Champagne is uncorked. Upon uncorking, the gas pressure in the bottle drops down to ambient values. The pressure difference of $\Delta P = P_{CO_2} - P_{ambient} = 4$ atm (4×10^5 Pa), a bottleneck cross-section of $A = 4 \times 10^{-4}$ m^2, and the cork mass $m_c = 10$ g and length of $L = 0.01$ m yield the kinetic energy $\frac{1}{2}m_cV^2 = \Delta PAL = 1.6$ J. Consequently, the velocity of cork popping out of a bottle can reach $V \approx 17.8$ m s^{-1} or 64.4 km h^{-1}.[6,8–10]

The rapid pressure drop facilitates an adiabatic expansion governed by

$$P^{(1-\Gamma)}T^{\Gamma} = \text{const} \quad (6)$$

where $\Gamma = 1.3$ is the ratio of specific heats, leading to the temperature drop by $5^{0.3/1.3} = 1.448$ times or by almost 90° at 290 K. The fog is often observed for several seconds near the neck of an open bottle due to the adiabatic cooling below the dew point.

The physicochemical parameters relevant to bubbles in pure water, pure ethanol, water–ethanol 12.5% solution, and sparkling wine are presented in Table 2.

Bubbles in the wine cup

The static equilibrium radius of a bubble is $R_e = \frac{2\gamma}{\Delta P}$, as given by the Laplace equation. Nucleation of the bubble and its collapse are metastable processes so that the liquid and bubble states are separated by a small energetic barrier. Under the harmonically oscillating ultrasound, the pressure $\Delta P = \Delta P_0 + A \cos \Omega t$ reaches negative values when at a minimum so that the bubble passes through the tensile and compressive stages.[2]

Bubbles tend to stick to the surface. Artificial effervescence is related to bubbles nucleated from glasses with imperfections done intentionally by the glassmaker to promote or eventually replace a deficit of natural nucleation sites. Thus, in plastic cups, gas desorption happens through heterogeneously nucleated CO^2 bubbles.[7]

In this section, we have seen that physical and physicochemical models of bubble formation can provide insights into such characteristics as density, viscosity, and carbon dioxide concentration. However, it is not possible to directly distinguish between different types of wine, such as rosé and white, or the type of glass. We hypothesize that CV and ML/AI methods allow for distinguishing these characteristics. Since the rate of natural bubbling decreases within minutes after uncorking, we will also the effect of time for which wine was exposed to air within a given type of glass (cup).

Experimental and computational method

Samples and equipment

Two types of sparkling wine, Rosé and White (produced by *Vysokiy Bereg*, Kuban' Region, Russia) were used for samples. Two types of wine glasses (cups) – one made out of glass and one made out of plastic – were used (Fig. 1(A)).

Experimental procedure

The bottles were uncorked and wine was placed into glass and plastic wine glasses (cups) for bubble formation, where they were kept for 10, 15, and 20 minutes (Fig. 1(B) and (C)). The choice of these time intervals was based on the observation that after 15–20 minutes of staying in an open wineglass, bubbling intensity decreases. The control measurement was also conducted immediately after opening the bottles (at 0 minutes). The samples were then poured into the Petri dishes and ultrasound cavitation bubbles were generated, which were recorded for video (Fig. 1(D)).

The working hypothesis was that bubble formation is different in glass and plastic cups due to the presence of centers of nucleation, such as scratches, at the plastic cup surface, as opposed to the relatively smooth glass.[7] The intensity of bubble

Table 2 Physicochemical parameters of water, champagne, and ethanol at 20 °C

	Water	Ethanol	Water–ethanol 12.5% mixture	Champagne[2]
Density, kg m^{-3}	1000	789	975	998
Viscosity, mPa s	1.002	1.14	1.48	1.48
Surface tension, mN m^{-1}	72	22	50	48
CO_2 pressure, atm	0	0	0	5–7
Critical radius of droplets, $R_{cr} = \frac{2\gamma}{P}$, mm	1.44	0.44	1.0	0.2

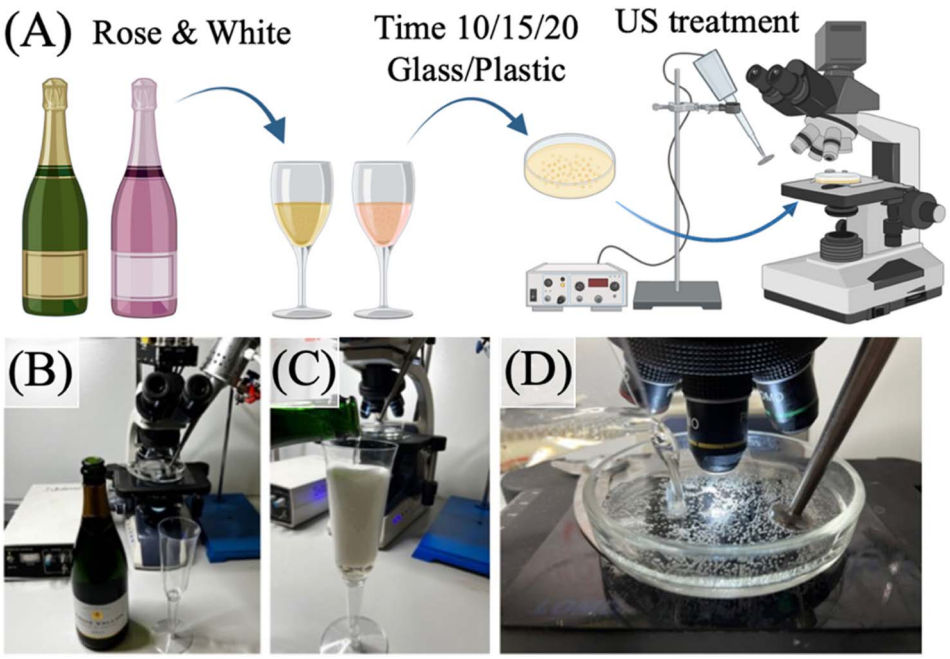

Fig. 1 (A) Schematic of the experimental procedure. (B) Two types of wine (C) were kept in glass and plastic cups and then (D) treated with ultrasound (US).

formation decreases after some time following uncorking the bottle. For that end, different time intervals, up to 20 minutes, were used.

To generate cavitation bubbles, the ultrasonic generator UZG 55-22 (BSUIR, Belarus) with a nominal rated frequency of 22 kHz and a nominal maximum power of 100 W was used. Ultrasonic oscillations were generated by the titanium sonotrode. The titanium sonotrode shaped as a truncated cone with a disk (15 mm diameter, 2 mm thickness) at the edge was positioned at the angle of 45° to the surface of a glass Petri dish filled with the wine being studied. The immersion depth was adjusted to ensure that the entire disk was fully submerged in the sample liquid.

The images of cavitation bubbles were recorded with the high-speed camera Phantom Miro C110, connected to the microscope Mikmed-6 (LOMO, Russia) with a 10× objective. The capturing frequency was 700 fps with a resolution of 768 × 768 px. The image set was automatically composed from the frame images as a single video file. The video file was edited with the application Phantom CV 3.3 to identify sections containing bubble formation, evolution, and collapse for each sample. In the past, the 12.5% water–ethanol solution was studied with the same methodology.[11]

Software & hardware

The primary stages of data processing and model training were implemented using Python 3.10 and specialized libraries. Specifically, the YOLOv8 model was utilized for image segmentation, while pytorch_tabnet was employed for data classification. Embedding generation was performed using Transformers, and basic data processing was conducted with OpenCV, NumPy, and auxiliary tools.

The computations were carried out on an AMD Ryzen Threadripper 3960X processor. To accelerate the training of neural networks, an NVIDIA GeForce RTX 3090 GPU was used, enabling fast computation of complex models and handling large volumes of data. This configuration facilitated the efficient execution of the entire data analysis cycle, from preliminary image processing to training and testing of advanced machine learning architectures.

Dataset

For the study, a dataset was created and structured, including visual data on cavitation bubbles in sparkling wine samples. The source data consisted of a collection of video recordings organized into directories based on a combination of characteristics: wine type (white or rosé), container type (glass or plastic), and time elapsed since the bottle was opened. This data structure allowed for clear systematization and classification of the information, which was a critical step in preparing the data for processing.

Data Processing Stages:

(1) Video segmentation

For preliminary video processing, the YOLOv8 segmentation model was employed, enabling efficient image processing by isolating frames containing cavitation bubbles. We utilized pretrained YOLOv8 weights from the study,[12] which significantly accelerated the integration of the model into the pipeline. After identifying the bubbles, their contours were outlined as polygons generated by the model. This step was added to the processing workflow following a series of experiments that demonstrated the contouring of polygons improved the classification model's accuracy by enhancing the quality of extracted features.

(2) Data splitting

After segmentation, the data was divided into training (60%), validation (20%), and test (20%) sets. This data distribution was chosen to ensure balanced model training and objective performance evaluation. This step minimizes the risk of overfitting and ensures that the test data remains completely independent of the training phase.

(3) Frames extraction

To reduce the data volume and improve processing efficiency, the videos were split into individual frames at a rate of 1 frame per 10 seconds. This approach preserved key temporal patterns, ensuring the data's representativeness for subsequent analysis.

Final dataset volume

- Train: 12 895 images
- Validation: 3744 images
- Test: 3314 images
- Total: 19 953 images

The use of YOLOv8 with pre-trained weights,[12] along with the added step of polygon contouring for detected bubbles, improved the data quality for classification. This approach enabled the extraction of more precise visual features, positively impacting the overall performance of the model. The general pipeline is presented in Fig. 2.

Computational pipeline

An iterative approach was used to develop the computational pipeline, drawing on experience from previous studies and testing various models. The final pipeline is presented in Fig. 2.

In the initial stages of the study, classical CNNs, such as VGG16, VGG19, ResNet18, and ResNet50, were employed for feature extraction. These models demonstrated good results but were limited in capturing complex relationships due to the lack of semantic context. This limitation motivated the integration of more advanced methods, such as CLIP.

Contrastive Language-Image Pretraining (CLIP)[20] marked the next stage in the evolution of the pipeline. CLIP enables the extraction of embeddings that combine both visual and semantic features of images, making the model more robust to noise in the data. Paired with the TabNet classifier,[21] CLIP demonstrated superior performance. TabNet was chosen for its ability to efficiently process embeddings while preserving model interpretability.

To improve classification quality, a TabNet Pretrainer was added, which was trained in an unsupervised mode to uncover hidden structures in the data. This allowed the model to better adapt to the characteristics of the embeddings, resulting in increased accuracy on the test dataset.

To further enhance feature quality, CLIP was replaced with its improved version, SigLIP.[22] The primary advantage of SigLIP lies in its expanded embedding space, enabling the model to capture more information from the images. Combined with TabNet and the TabNet Pretrainer, this approach proved to be the best among all tested methods.

At the final stage, all images containing cavitation bubbles were processed through the segmentation model, followed by embedding extraction using SigLIP (Fig. 2). The embeddings served as input for the TabNet Pretrainer, which structured the data, and the TabNet Classifier, which performed the final classification. This approach achieved maximum accuracy and classification stability.

Results and discussion

Typical shapes of cavitation bubbles are shown in Fig. 3(A). The bubbles obtained by the ultrasound cavitation (20 kHz) were compared with those without cavitation used as controlled experiments. The bubbles for the four experimental series, with waiting periods from 0 minutes to 20 minutes are shown in Fig. 3(B).

It is observed that based on the visual analysis it is very difficult to find the difference between different series in the cavitation experiments.

The classification accuracy evaluation is presented in Fig. 4(A) and (B) as normalized confusion matrices. These matrices depict the results of two primary classification tasks: the type of champagne (rosé or white) and the type of glass (glass or plastic).

Fig. 4(A) shows the confusion matrix for the classification of rosé (pink) and white champagne. The overall classification accuracy for this task was 84%. While the model exhibits a strong ability to distinguish between the two types of champagne, an error rate of 14–15% persists due to visual similarities

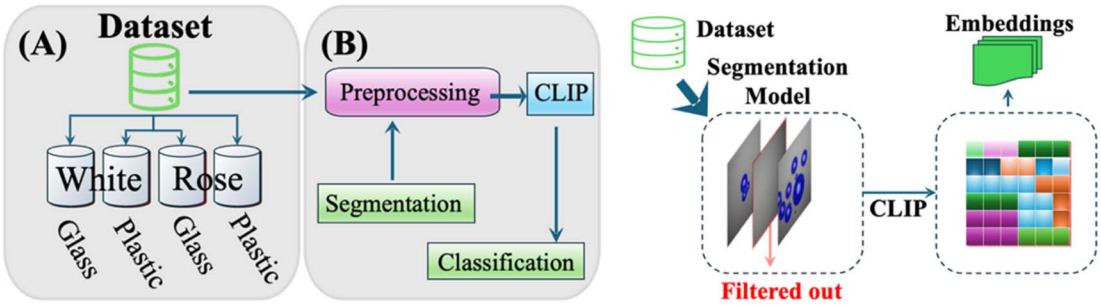

Fig. 2 The pipeline for the classification of sparkling wines. (A) The structure of the dataset contains two types of wine and two types of containers. (B) The scheme of preprocessing classification model. All images containing bubbles pass through the SigLIP network converting to embeddings used for training the ML algorithm.

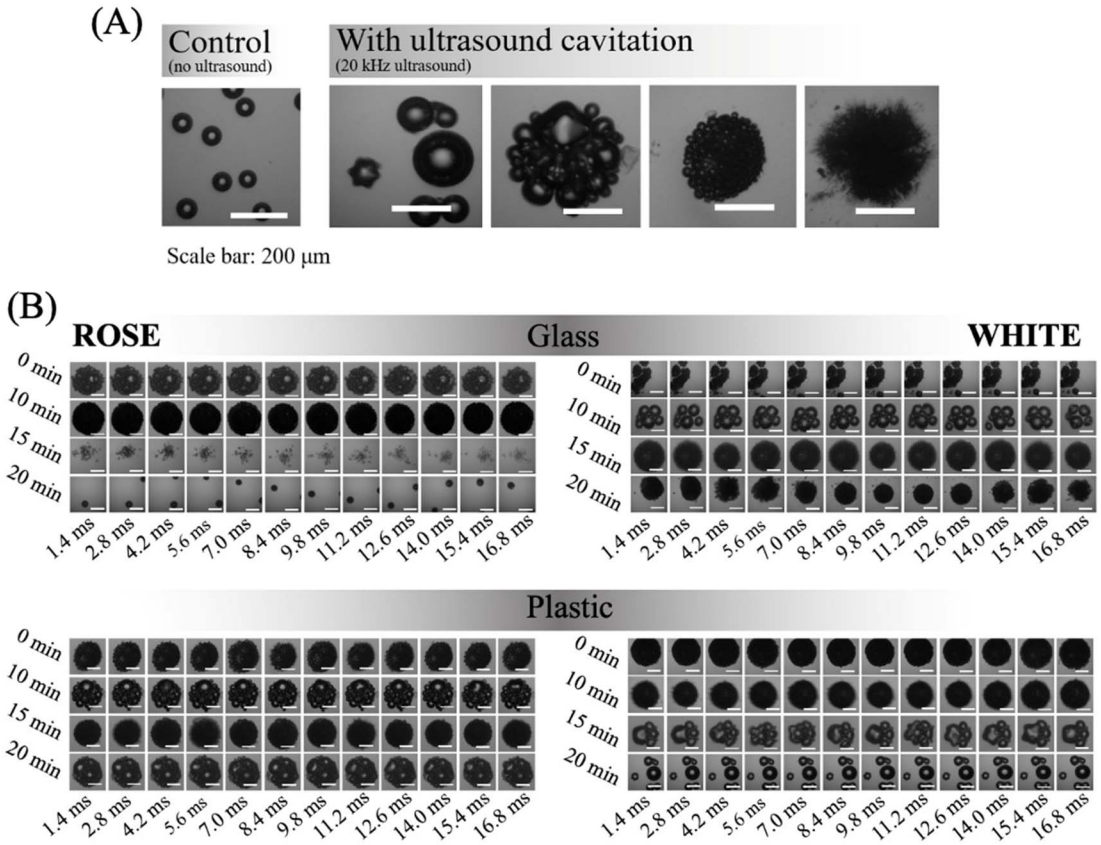

Fig. 3 (A) Typical bubbles in the control series (no ultrasound) and in the cavitation series. (B) Bubbles in various experimental series.

in the bubble patterns characteristic of different wine types. This highlights the limitations of classification tasks based solely on visual data.

Fig. 4(B) presents the confusion matrix for the classification of container types: glass (glass) or plastic (plastic). The overall accuracy for this task was 82%. While the model demonstrated a good ability to differentiate between containers, the error rate of 15–20% suggests that the surface properties of the containers, which influence bubble behavior, may require more detailed analysis or additional data processing to improve the results.

The obtained confusion matrices demonstrate the high efficiency of the proposed pipeline for both classification tasks. However, the accuracy rates of 84% for champagne classification and 82% for container type classification indicate potential areas for improvement. For instance, incorporating temporal dynamics from the videos or enhancing the data preprocessing stage (*e.g.*, contrast enhancement or additional normalization techniques) could help reduce the error rate.

The use of SigLIP[22] as a feature extractor played a key role in achieving these results. Its enhanced embedding space provided richer and more informative features compared to previously employed methods. Additionally, the integration of TabNet[21] as the classifier enabled effective processing of complex embedding and tabular data. These innovations significantly improved classification accuracy compared to

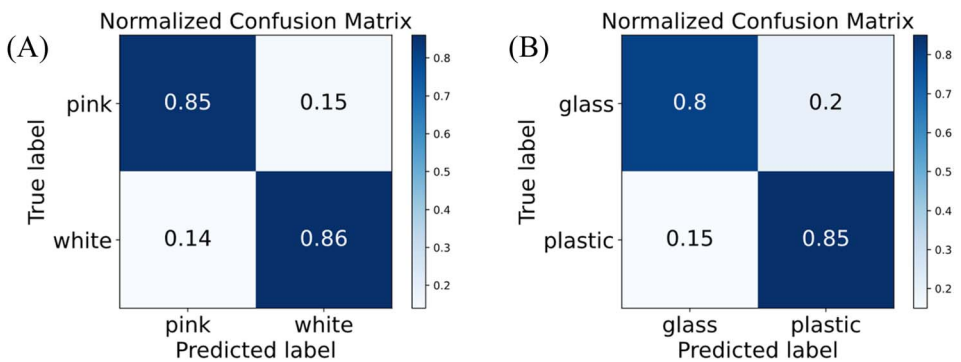

Fig. 4 Confusion matrices for (A) the two types of sparkling wine and (B) two types of containers.

earlier versions of the pipeline, affirming the validity of the chosen approach.

It is interesting to compare bubble dynamics in sparkling wines with that of other carbonated beverages, such as beer and sodas. According to Bossaerts *et al.*, the properties of bubbles in beer depend strongly on the concentration of alcohol (non-alcoholic beers have fewer bubbles) and is affected strongly by the CO_2 concentration and the surface tension, which, in turn, is dependent on alcohol, protein, and iso-alpha-acid content in beer.[23] An explicit comparison of bubbling dynamics in champagne wines and beers[24] shows that the critical radius of bubbles in beers is about twice as that in champagne due to higher concentration of dissolved CO_2 in champagne. As far as other carbonated liquids, the bubble generation is promoted by hydrophilic structures on container's surface and suppressed by hydrophobic structures.[25] These insights suggest that different carbonated beverages are characterized by different bubbling behavior, which is consistent with our observation on rosé and white sparkling wine.

Conclusion

The results indicate the feasibility of using computer vision algorithms for the analysis of cavitation bubbles in carbonated beverages. It was possible to classify the samples based on the type of beverage and type of glass. However, it is much more difficult to determine other characteristics, such as the exposure time for open air. We conclude that ultrasonic bubble cavitation can be used for the study of the physicochemical properties of various transparent liquids including carbonated sparkling beverages.

Data availability

The code and data used in this study are available in the GitHub repository at **https://github.com/ShockOfWave/bubbles_champagne**. This repository contains the source code used for the analysis, as well as the datasets utilized for training and testing the model. Researchers interested in replicating or extending this study can access the repository to review the code implementation and perform further analyses.

Conflicts of interest

There are no conflicts to declare.

Acknowledgements

The research was carried out within the state assignment of the Ministry of Science and Higher Education of the Russian Federation (project No. FSER-2024-0003).

References

1 Anonymous. Sparkling Wine Market by Type, Product, Price Point, and Sales Channel: Opportunity Analysis and Industry Forecast, 2021–2027 (Allied Market Research, 2021), **https://www.alliedmarketresearch.com/sparkling-wines-market-A08370**.

2 G. Liger-Belair, The Physics and Chemistry behind the Bubbling Properties of Champagne and Sparkling Wines: A State-of-the-Art Review, *J. Agric. Food Chem.*, 2005, **53**, 2788–2802.

3 G. Liger-Belair, G. Polidori and P. Jeandet, Recent advances in the science of champagne bubbles, *Chem. Soc. Rev.*, 2008, **37**, 2490–2511.

4 G. Liger-Belair, F. Beaumont, M. Bourget, H. Pron, B. Parvitte, V. Zéninari, G. Polidori and C. Cilindre, "Carbon Dioxide and Ethanol Release from Champagne Glasses, Under Standard Tasting Conditions" 2012, in *Advances in Food and Nutrition Research*, ed. J. Henry, Academic Press, 2012, vol. 67, pp. 289–340, DOI: **10.1016/B978-0-12-394598-3.00007-1**.

5 M. Vignes-Adler, The Fizzling Foam of Champagne, *Angew. Chem., Int. Ed.*, 2013, **52**, 187–190, DOI: **10.1002/anie.201207299**.

6 G. Liger-Belair, M. Bourget, C. Cilindre, *et al.*, Champagne cork popping revisited through high-speed infrared imaging: The role of temperature, *J. Food Eng.*, 2013, **116**(1), 78–85.

7 G. Liger-Belair, F. Sternenberg, S. Brunner, B. Robillard and C. Cilindre, Bubble dynamics in various commercial sparkling bottled waters, *J. Food Eng.*, 2015, **163**, 60–70.

8 G. Liger-Belair, D. Cordier, J. Honvault, *et al.*, Unveiling CO2 heterogeneous freezing plumes during champagne cork popping, *Sci. Rep.*, 2017, **7**, 10938, DOI: **10.1038/s41598-017-10702-6**.

9 G. Liger-Belair, D. Cordier and R. Georges, Under-expanded super-sonic CO2 freezing jets during champagne cork popping, *Sci. Adv.*, 2019, **5**(9), eeav5528, DOI: **10.1126/sciadv.aav5528**.

10 A. Benidar, R. Georges, V. Kulkarni, *et al.*, Computational fluid dynamic simulation of the supersonic CO_2 flow during champagne cork popping, *Phys. Fluids*, 2022, **34**, 066119.

11 I. Korolev, T. A. Aliev, T. Orlova, S. A. Ulasevich, M. Nosonovsky and E. V. Skorb, When bubbles are not spherical: artificial intelligence analysis of ultrasonic cavitation bubbles in solutions of varying concentrations, *J. Phys. Chem. B*, 2022, **126**(16), 3161–3169.

12 T. A. Aliev, I. Korolev, O. Burdulenko, E. Alchinova, A. Subbota, M. Yasnov, M. Nosonovsky and E. V. Skorb, Automatic image processing of cavitation bubbles to analyze properties of petroleum products, *Digital Discovery*, 2024, **3**, 1101–1107.

13 M. Ashokkumar, The characterization of acoustic cavitation bubbles – An overview, *Ultrason. Sonochem.*, 2011, **18**(4), 864–872, DOI: **10.1016/j.ultsonch.2010.11.016**.

14 S.-W. Ohl, E. Klaseboer and B. C. Khoo, Bubbles with shock waves and ultrasound: a review, *Interface Focus*, 2015, **5**(5), 20150019, DOI: **10.1098/rsfs.2015.0019**.

15 M. Hauptmann, F. Frederickx, H. Struyf, P. Mertens, M. Heyns, S. De Gendt, C. Glorieux and S. Brems, Enhancement of cavitation activity and particle removal

with pulsed high frequency ultrasound and supersaturation, *Ultrason. Sonochem.*, 2012, **20**, 69–76, DOI: **10.1016/j.ultsonch.2012.04.015**.

16 M. Guédra, S. Cleve, C. Mauger, P. Blanc-Benon, C. Inserra and C. Dynamics, of nonspherical microbubble oscillations above instability threshold, *Phys. Rev. E*, 2017, **96**, 063104.

17 S. Shityakov, E. V. Skorb and M. Nosonovsky, TAS2R taste receptor clustering suggests that bitter wine taste perception forms a 2D dataspace, *J. Comput. Biophys. Chem.*, 2025, DOI: **10.1142/S2737416524500844**.

18 M. S. Ashikhmina, A. M. Zenkin, I. S. Pantiukhin, I. G. Litvak, P. V. Nesterov, K. Dutta, *et al.*, Uncovering the taste features: Applying machine learning and molecular docking approaches to predict umami taste intensity of peptides, *Food Biosci.*, 2024, **62**, 105358.

19 A. C. Muñoz-Espada, *et al.*, Anthocyanin Quantification and Radical Scavenging Capacity of Concord, Norton, and Marechal Foch Grapes and Wines, *J. Agric. Food Chem.*, 2004, **52**(22), 6779–6786, DOI: **10.1021/jf040087y**.

20 H.-Y. Chen, Z. Lai, H. Zhang, X. Wang, M. Eichner, K. You, M. Cao, B. Zhang, Y. Yang and Z. Gan, Contrastive Localized Language-Image Pre-Training, *arXiv*, 2024, preprint, arXiv:2410.02746, DOI: **10.48550/arXiv.2410.02746**, Retrieved from **https://arxiv.org/abs/2410.02746**.

21 M. Joseph, PyTorch Tabular: A Framework for Deep Learning with Tabular Data, *arXiv*, preprint, 2021, arXiv:2104.13638, DOI: **10.48550/arXiv.2104.13638**, Retrieved from **https://arxiv.org/abs/2104.13638**.

22 X. Zhai, B. Mustafa, A. Kolesnikov and L. Beyer, Sigmoid Loss for Language Image Pre-Training, in *2023 IEEE/CVF International Conference on Computer Vision (ICCV)*, Paris, France, 2023, pp. 11941–11952, DOI: **10.1109/ICCV51070.2023.01100**.

23 L. Bossaerts, F. Van Opstaele, A. G. B. Wouters, C. M. Courtin and N. A. Langenaeken, Study of the influence of beer composition on the amount of bubbles in beer: CO2, alcohol, protein and iso-alpha-acid contents as primary predictors, *Food Chem.*, 2025, **469**, 142523, DOI: **10.1016/j.foodchem.2024.142523**.

24 G. Liger-Belair and C. Cilindre, How Many CO2 Bubbles in a Glass of Beer?, *ACS Omega*, 2021, **6**(14), 9672–9679, DOI: **10.1021/acsomega.1c00256**.

25 J.-W. Lee, S. Kim, S. Lee and W. Hwang, Exponential promotion and suppression of bubble nucleation in carbonated liquid by modification of surface wettability, *Appl. Surf. Sci.*, 2020, **512**, 145709, DOI: **10.1016/j.apsusc.2020.145709**.